Theor Chim Acta (1985) 68: 23-44

An *ab initio* potential energy surface and dynamics calculations for vibrational excitation of I_2 by He

Franklin B. Brown, David W. Schwenke, and Donald G. Truhlar

Department of Chemistry, University of Minnesota, Minneapolis, Minnesota 55455, USA

(Received November 15, 1984)

We present new *ab initio* calculations of the interaction potential and the elastic and inelastic cross sections for He scattering by I_2. The electronic structure calculations of the interaction potential are based on an extensive one-electron basis set (triple zeta plus a *d* set on each I, an *s* function plus a *p* set at the I_2 bond center, and quadruple zeta plus two *p* sets on He), a two-configuration-SCF orbital set, and a configuration interaction calculation based on all single and double excitations out of the two-configuration reference space. The calculations are performed at 16He–I_2 distances for nine combinations of I_2 vibrational displacement and orientation. A new form of analytic representation is presented that is particularly well suited to efficient and accurate fitting of *ab initio* interaction potentials that include vibrational displacements. Scattering calculations are performed by the vibrational close-coupling, rotational-infinite-order-sudden approximation with a converged vibrational basis.

Key words: Multireference configuration interaction calculations — Non-pairwise additive potential surface — Vibrational-rotational scattering calculations

1. Introduction

Hall et al. [1] have recently reported the first measurement of the energy dependence of a vibrational excitation cross section for a collisional system involving uncharged species. The system they studied, He–I_2, has also been widely studied [2] with regard to predissociation of the van der Waals complex and vibrational energy transfer in non-energy-selected collisions, although the experiment of Hall et al. refers to the ground electronic state, and most previous work refers to I_2 in the $B^3\Pi_{0_u^+}$ excited electronic state. In the present paper we report a full potential energy surface for He–I_2 in the ground electronic state, with special emphasis

on those properties of the potential energy surface that are expected to have a strong effect on the vibrational excitation cross sections measured by Hall et al.

We have previously reported [3] a pairwise additive (PA) approximation to the potential energy surface for He-I_2 collisions that was based in part on *ab initio* calculations and in part on theoretical and experimental estimates of the long-range forces and the properties of the van der Waals complex. The PA potential was used for scattering calculations [4] and it yielded semiquantitative agreement with the experimental vibrational excitation cross sections; however, as compared to the experimental results, the calculations showed significantly more rotational excitation accompanying the vibrationally inelastic events. The discrepancy between the theoretical and experimental rotational-vibrational distributions was tentatively ascribed to incorrect anisotropy of the PA potential. In the present calculation we remove the assumption of pairwise additivity. The present potential also improves on the previous one in several other respects: (i) we use a more accurate effective core potential to treat the core electrons of I, (ii) we use a more extensive and well optimized one-electron basis set of gaussian functions, (iii) we use a two-configuration self-consistent-field (SCF) calculation to obtain the orbitals for a more complete configuration interaction (CI) treatment of electron correlation effects. In particular the present calculations treat electron correlation effects in terms of configuration mixing with all single and double excitations from an optimized-double-configuration (ODC) [5] reference state, whereas the previous calculations used a single-configuration reference and third-order Møller–Plesset perturbation theory. Point (iii) is considered particularly important because the vibrational excitation cross sections are expected [4, 6] to be particularly sensitive to the derivative of the interaction potential with respect to the I–I stretching coordinate and a multi-reference orbital set is required for a correct description of the wave function as this coordinate is increased. One might consider adding a fourth item to the above list, namely (iv) the present calculations are entirely *ab initio*; we realize however, that this need not lead to improved reliability.

In addition to reporting the new electronic structure calculations, we report an analytic representation of the potential energy surface by a new functional form that may be useful for non-PA approximations to other atom-diatom potential energy surfaces, and we report new dynamics calculations. Comparing the new dynamics calculations for the non-PA potential to the previous ones [4] for the PA potential [3] provides a test of the PA assumption. One general reason, in addition to the specific question mentioned above of rotational inelasticity, for quantitatively testing the PA approximation is its great appeal for constructing potential surfaces involving polyatomic molecules. Two examples closely related to the present study are the use of PA potentials for vibrational excitation of polyatomics in collisions with rare gases [7] and the use of PA potentials for pentacene-rare gas van der Waals molecules [8].

Section 2 discusses the electronic structure calculations, in particular (2.1) the choice of effective core potential, (2.2) the multi-reference SCF and CI procedures,

and (2.3) the choice of gaussian basis set. Section 3 presents the new method for the analytical representation of an A-BC interaction potential; in particular we present a fitting procedure that exactly reproduces the *ab initio* calculations at a finite number of BC orientation angles and also includes a qualitatively correct pairwise interaction when A gets very close to either B or C. Section 4 gives the details of the scattering calculations; Section 5 presents the results and discusses them. A particularly important point considered in the discussion section is what we have learned about the validity of the widely applied [2] PA approximation for interaction potentials in this kind of system. Section 6 contains concluding remarks.

2. *Ab initio* calculations

2.1. *Effective core potential*

Since HeI_2 has a very large number of electrons, we replace the core orbitals on I by an effective core potential (ECP) as was done in the previous calculations [3]. This reduces the number of electrons considered explicitly to 16, thus reducing one-electron basis set requirements and the size of the configuration interaction expansion substantially. As compared to our previous calculations though, the present calculations employ an improved ECP for I.

The ECP for I that was used in the first set of calculations [3] was determined by Kahn et al. [9] and was based upon a Phillips-Kleinman-like pseudo-orbital

Table 1. Effective core potentials[a] for I where the parameters are defined by $U_{ECP}=\sum_{k=1}^{5} d_{3k} r^{n_{3k}} \exp(-\alpha_{3k} r^2)+\sum_{l=0}^{2}\sum_{m=-l}^{l} |lm\rangle\langle lm| \sum_{k=1}^{5} d_{lk} r^{nlk} \exp(-\alpha_{lk} r^2)$

l	n_{lk}	α_{lk}(a.u.)	d_{lk}(a.u.)
3	0	1.0715702	−0.0747621
	1	44.1936028	−30.0811224
	2	12.9367609	−75.3722721
	2	3.1956412	−22.0563758
	2	0.8589806	−1.6979585
0	0	127.9202670	2.9380036
	1	78.6211465	41.2471267
	2	36.5146237	287.8680095
	2	9.9065681	114.3758506
	2	1.9420086	37.6547714
1	0	13.0035304	2.2222630
	1	76.0331404	39.4090831
	2	24.1961684	177.4075002
	2	6.4053433	77.9889462
	2	1.5851786	25.7547641
2	0	40.4278108	7.0524360
	1	28.9084375	33.3041635
	2	15.6268936	186.9453875
	2	4.1442856	71.9688361
	2	0.9377235	9.3630657

[a] Ref. [13].

transformation [9, 10]. However, Hay et al. [11] have shown that pseudo-orbitals determined by this method may have inaccurate tails, leading to ECP's that yield too large dissociation energies and too small bond lengths when compared to results from corresponding all-electron (AE) calculations. Christiansen et al. [12] have proposed a better method in which a given pseudo-orbital matches exactly the corresponding Hartree–Fock orbital, including the normalization, in the valence region. Thus the pseudo-orbitals differ from the Hartree–Fock orbitals only in the core region near the nuclei. Using this method, improved ECP's have been determined which give good agreement between ECP and AE calculations of bond lengths and dissociation energies [12]. Wadt and Hay [13] have used such pseudo-orbitals to obtain ECP's for most of the atoms in the periodic table, and we use their ECP for I in the present calculations. Relativistic effects are included implicitly in this ECP because it is based on orbitals obtained from the relativistic Hartree–Fock equations of Cowan and Griffen [14], which include "mass-velocity" and "Darwin" terms. This method has proven to be reliable when compared to more rigorous methods [15]. In summary the new ECP should be more reliable than the previous one since it contains relativistic effects and it correctly treats the normalization condition in the valence space. In addition the new ECP includes angular momentum projectors for *s*, *p*, and *d* orbitals, whereas the previous one included only *s* and *p* projectors. Table 1 lists the parameters used in the pseudopotential.

2.2. SCF *and* CI *methods*

The general technique used to calculate the electronic energy is the multi-reference configuration interaction method with single and double excitations (MR CISD) [16]. In this method we include all configurations that can be constructed by single or double excitations from a reference set of configurations, which in the present case consists of only the two configurations needed to properly describe the dissociation of I_2. Thus for I_2 the reference space consists of the ground-state configuration and the double excitation of 2 electrons from the highest occupied σ_g orbital to the lowest unoccupied σ_u orbital; this is $2\sigma_g^2 \rightarrow 2\sigma_u^2$ in the valence-electron number scheme. The generalizations for linear, C_{2v}, and non-symmetric geometries of HeI_2 are $4\sigma^2 \rightarrow 5\sigma^2$, $4a_1^2 \rightarrow 3b_2^2$, and $6a'^2 \rightarrow 7a'^2$. Having these excited configurations in the reference space allows for a more accurate description of the I_2 stretching motion for all geometries.

The techniques used for optimizing molecular orbitals for the two-configuration reference space are explained elsewhere (multi-configuration self-consistent-field method [17]), and these calculations as well as the MR CISD calculations were carried out using the COLUMBUS programs [18].

2.3. One-electron basis set

In choosing a one-electron basis set to use in the present calculations, we established three criteria which the calculated potential energy surface should satisfy and we optimized and enlarged the basis set until these criteria were met.

In order of decreasing importance, the criteria are: (i) The basis set should be sufficiently complete that the stretching potential of the isolated I_2 molecule is described well. (ii) The bond-stretching force, $-\partial V_{int}/\partial r$, evaluated at $r = r_e$, where V_{int} is the interaction energy of He and I_2, r is the distance between the two I atoms, and r_e is the equilibrium value of r, should be well converged with respect to changing the basis set. (iii) The calculated equilibrium structure of the HeI_2 van der Waals (vdW) complex should agree reasonably well with the experimentally determined structure [19, 20]. In particular, for (iii), we required that the potential well of the bent or T-shaped HeI_2 complex should be deeper than or at least comparable to that of the collinear complex since the prevailing interpretation of the experimental data supports a vibrationally averaged nonlinear structure for the vibrational ground state [19].

For I, we begin with an *sp* basis set, which is listed in Table 2, from Wadt and Hay [13]. In order that the computed value of r_e for I_2 reproduce the experimental value of 5.039 a_0 [21], one set of nuclear-centered *d*-type functions was added at each I, and one *s*-type and one set of *p*-type functions were added at the bond center. The exponential parameters for the *d* functions and the bond-centered functions were chosen to reproduce r_e within 0.015 a_0 at the MR CISD level and are also given in Table 2. The final basis yields $r_e = 5.054$ a_0. In addition it yields a harmonic stretching frequency of 220.0 cm^{-1}, as compared to the experimental value [21] of 214.5 cm^{-1}.

Table 2. Gaussian basis set [3*s*3*p*1*d*/1*s*1*p*/4*s*2*p*] used in present calculations

Center	Symmetry	Exponential parameter (a.u.)	Contraction coefficient[a]
I	*s*	0.7242	1.0
I	*s*	0.4653	1.0
I	*s*	0.1336	1.0
I	*p*	1.2900	1.0
I	*p*	0.3180	1.0
I	*p*	0.1053	1.0
I	*d*	0.275	1.0
B[b]	*s*	0.52	1.0
B[b]	*p*	0.52	1.0
He	*s*	414.46650	0.001272
		62.24915	0.009712
		14.22123	0.047271
		4.038781	0.158146
He	*s*	1.297177	1.0
He	*s*	0.44753	1.0
He	*s*	0.160274	1.0
He	*p*	1.3	1.0
He	*p*	0.25	1.0

[a] Coefficient of primitive basis function.
[b] B denotes bond midpoint of I_2.

The *s* basis set for He is taken from Huzinaga [22] and is one of the bases employed by Meyer et al. [23] in their study of HeH_2. Two sets of *p*-type polarization functions are added to the He *s* basis. We found that the interaction energy in the vdW well region is quite sensitive to the choice of exponential parameter of the diffuse *p* set. In particular the interaction energy varies by 300% when the exponential parameter of the diffuse *p* function on He is varied in the range 0.1–0.5 a.u.. In contrast the same interaction energy is quite insensitive to the exponential parameter chosen for the tighter *p* function. Thus the tight *p* exponential parameter was optimized in a configuration interaction calculation (all single and double excitations from a single-configuration Hartree–Fock reference, which, for He, corresponds to a full CI calculation in the given one-electron basis) on atomic He; this yields 1.3 a.u.. Ideally the diffuse *p* exponential parameter would be chosen to optimize the electronic energy of the vdW complex. However a converged calculation of the vdW binding energy and geometry would require an extremely well balanced treatment of correlation errors in the complex and the separated subsystems and is probably beyond the state of the art. Thus we settled for a more empirical approach in which the diffuse *p* exponential parameter was chosen to make the calculated geometry (R_e, which denotes the distance from the center of mass of I_2 to He at the local minimum) and binding energy (D_e) of the T-shaped vdW complex close to the estimated values of Ref. [3] and to insure that the calculated binding energy of the linear vdW complex is not significantly greater. By trial and error we thus settled on a diffuse *p* exponential parameter of 0.25 a.u., which yields $R_e = 7.82$ a_0 and $D_e = 2.69$ meV for the T-shaped complex and $R_e = 9.94$ a_0 and $D_e =$ 2.78 meV for the linear one, with a saddle point between these local minima. Thus the collinear complex is calculated to be more stable than the perpendicular complex by only 0.09 meV.

Admittedly, as discussed above, we have not converged the potential surface in the region of the vdW well with respect to the basis set; however, the goal of the present calculations is the creation of a potential surface that is useful for $He + I_2$ scattering calculations at relative translational energies much greater than the vdW well depth, and such calculations are primarily sensitive to the repulsive wall of the potential and the bond-stretching force at geometries corresponding to highly repulsive interactions [4]. Thus we think that any reasonable description of the vdW well is adequate for the present purposes.

Table 3 reports a special set of calculations designed to illustrate the degree of basis-set independence of the bond-stretching force ($-\partial V_{\text{int}}/\partial r$) at energies near 0.1 eV, which is the energy for which scattering calculations are reported in Section 4. For completeness, Table 3 also shows some of the results for V_{int} in the vdW region. Since the I_2 basis set is chosen to make r_e correct for isolated I_2, Table 3 only shows the sensitivity of V_{int} and $-\partial V_{\text{int}}/\partial r$ to the He basis. For this table, for a given value of R, the magnitude of the vector $\vec{R}$ from the center of mass of I_2 to He, and χ, the angle between the I_2 axis and $\vec{R}$, and r, the distance between the two I atoms, the force is obtained by calculating V_{int} at $r = 4.854$, 5.054, and 5.254 a_0, fitting it to a parabola, and analytically evaluating the derivative at $r = 5.054$ a_0.

Table 3. Dependence of the interaction potential (V_{int}) and the bond-stretching force ($-\partial V_{int}/\partial r$) on the He basis set

s basis[a]	p basis α_1(a.u.)	p basis α_2(a.u.)	R (a_0)	V_{int} (meV)[b]	$-\partial V_{int}/\partial r$ (meV/a_0)
			perpendicular HeI_2 ($\chi = 90°$)		
1	1.3	0.10	5.0[c]	120.5	20.1
1	1.3	0.25	5.0	117.8	17.4
1	1.3	0.50	5.0	130.2	19.3
1	1.3	0.10	8.0[d]	−5.33	—
1	1.3	0.25	8.0	−2.67	—
1	1.3	0.50	8.0	−1.77	—
1	1.5	0.25	8.0[d]	−2.67	—
1	1.3	0.25	8.0	−2.67	—
1	1.0	0.25	8.0	−2.69	—
			collinear HeI_2 ($\chi = 0°$)		
1	1.3	0.10	7.5[c]	105.6	−111.3
1	1.3	0.25	7.5	100.4	−103.3
1	1.3	0.50	7.5	106.9	−106.1
1	1.5	0.25	7.5[c]	100.1	−103.1
1	1.3	0.25	7.5	100.4	−103.3
1	1.0	0.25	7.5	100.1	−103.5
1	1.3	0.25	7.5[c]	100.4	−103.3
2	1.3	0.25	7.5	99.0	−103.2

[a] See text for definition of s basis sets.
[b] V_{int} is defined as the difference between the potential energy at a given I–I distance r, I_2–He distance R, and orientation angle χ (the angle between the I_2 axis and the vector from the center of I_2 to He) and the potential energy at the same r and χ with $R = 20.0\ a_0$. The value of r is $5.054\ a_0$ for all entries in this table.
[c] Repulsive wall region of the potential energy surface.
[d] vdW well region of the potential energy surface.

First consider the s basis and the exponential parameter of the tight p set on He. The s basis was varied by replacing the s basis of Table 2 by the 311 basis of Pople et al. [24] augmented by a diffuse s function with an exponential parameter of 0.08 a.u. In Table 3, the s basis of Table 2 is called basis 1 and the augmented 311 basis is called basis 2. The tight p set on He was varied by simply changing the exponential parameter, called α_1 in Table 3. Table 3 shows that $-\partial V_{int}/\partial r$ is very insensitive to changes in these aspects of the basis set. Next consider the variation of the exponential parameter, called α_2 in Table 3, of the diffuse p set on He. Table 3 shows that the bond-stretching forces vary by 16% or less when the exponential parameter of the diffuse p set on He is varied by a factor of 5, even though V_{int} of the T-shaped complex, with a fixed R near the vdW minimum, varies by a factor of 3.0 (1.77–5.33 meV) for the same exponential-parameter range.

We conclude from the discussions above that the basis set given in Table 2 satisfies the three criteria established at the beginning of this section. Thus, this basis set was used in the MR CISD calculations.

In actually performing the MR CIDS calculations, the COLUMBUS programs only explicitly take advantage of the symmetry elements of the C_{2v} and C_s point groups, as appropriate to the given HeI_2 geometry. For the basis set given in Table 2, this yields 28 218 and 53 623 spin and symmetry-adapted configurations for $C_{\infty v}$ or C_{2v} and C_s geometries respectively.

The final result of the *ab initio* calculations is a set of interaction potentials, calculated as

$$V_{\text{int}}(r, R, \chi) = E_{HeI_2}(r, R, \chi) - E_{HeI_2}(r, R = 20\ a_0, \chi)$$

where E_{HeI_2} is the total calculated energy at a given geometry (r, R, χ) where r is the diatom vibrational separation, R is the magnitude of the vector $\vec{R}$ from

Table 4. MR CISD interaction energies on HeI_2 potential energy surface[a]

R (a_0)	V_{int} ($r = 4.854\ a_0$) (meV)	V_{int} ($r = 5.054\ a_0$) (meV)	V_{int} ($r = 5.254\ a_0$) (meV)
		perpendicular HeI_2 ($\chi = 90°$)	
3.0	2.79 (3)[b]	2.59 (3)	2.39 (3)
4.0	6.65 (2)	6.31 (2)	5.95 (2)
5.0	1.21 (2)	1.18 (2)	1.14 (2)
6.0	1.15 (1)	1.23 (1)	1.27 (1)
7.0	−2.61	−2.20	−1.93
7.5	−2.99	−2.83	−2.78
8.0	−2.67	−2.67	−2.67
8.5	−2.15	−2.18	−2.23
9.0	−1.16	−1.63	−1.66
9.5	−1.14	−1.14	−1.17
10.0	−0.76	−0.76	−0.79
10.5	−0.52	−0.52	−0.52
11.0	−0.35	−0.35	−0.35
12.0	−0.19	−0.19	−0.19
13.0	−0.11	−0.11	−0.11
20.0	0.00	0.00	0.00
		collinear HeI_2 ($\chi = 0°$)	
3.0	5.10 (5)	6.54 (5)	8.71 (5)
4.0	5.06 (4)	6.34 (4)	7.96 (4)
5.0	7.16 (3)	8.58 (3)	9.58 (3)
6.0	1.42 (3)	1.64 (3)	1.89 (3)
7.0	2.31 (2)	2.76 (2)	3.30 (2)
7.5	8.17 (1)	1.00 (2)	1.23 (2)
8.0	2.39 (1)	3.11 (1)	4.00 (1)
8.5	3.51	6.01	9.20
9.0	−2.39	−1.71	−0.79
9.5	−3.27	−3.18	−3.05
10.0	−2.69	−2.78	−2.86
10.5	−1.96	−2.04	−2.15
11.0	−1.36	−1.44	−1.55
12.0	−0.68	−0.71	−0.76
13.0	−0.33	−0.35	−0.38
20.0	0.00	0.00	0.00

Table 4. (cont.)

R (a_0)	V_{int} (r=4.854 a_0) (meV)	V_{int} (r=5.054 a_0) (meV)	V_{int} (r=5.254 a_0) (meV)
		bent HeI_2 with χ=45°	
3.0	1.75 (4)	1.65 (4)	1.54 (4)
4.0	8.09 (3)	8.04 (3)	7.61 (3)
5.0	2.25 (3)	2.36 (3)	2.46 (3)
6.0	5.01 (2)	5.37 (2)	5.73 (2)
7.0	9.07 (1)	9.93 (1)	1.08 (2)
7.5	3.45 (1)	3.84 (1)	4.25 (1)
8.0	1.13 (1)	1.30 (1)	1.47 (1)
8.5	2.34	3.05	3.76
9.0	−0.84	−0.57	−0.30
9.5	−1.77	−1.69	−1.61
10.0	−1.77	−1.77	−1.77
10.5	−1.44	−1.47	−1.50
11.0	−1.03	−1.06	−1.12
12.0	−0.46	−0.46	−0.49
13.0	−0.22	−0.22	−0.22
20.0	0.00	0.00	0.00

[a] V_{int}, r, R, and χ are defined in footnote b of Table 3.
[b] Numbers in parentheses are multiplicative powers of ten.

the center of the I_2 moiety to He, and χ is the angle between the I_2 axis and $\vec{R}$. These interaction energies are given in Table 4.

Figure 1 compares the present calculations for the perpendicular bisector approach to those of Ref. [3]. The figure shows large differences in the vdW well region and hence in the outer, bottom reaches of the repulsive wall. The region most important for the vibrational excitation experiments of Ref. [1] is estimated

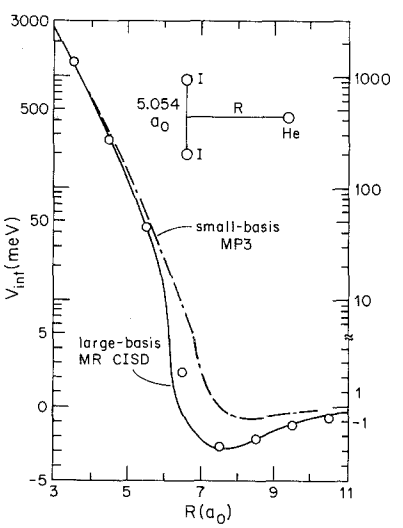

Fig. 1. Interaction potential for the He-I_2 in the perpendicular bisector geometry with $r = r_e$. The curves are the *ab initio* calculations of Ref. [3] and the present paper. The circles, given at 1.0 a_0 intervals from 3.5 to 10.5 a_0, are the final partly empirical analytic potential of Ref. [3]. Notice that, as is usual for this kind of plot, the ordinate scale is linear near the bottom and logarithmic near the top

to be where the potential is about 40–450 meV. Figure 1 shows much better convergence in that range and absolutely excellent agreement at even shorter range where the interaction potential exceeds 500 meV. Since the two sets of calculations are based on different ECP's and different methods of including electron correlation, this good agreement gives us added confidence in both these aspects of the calculation. In Ref. [3] we recognized the incomplete convergence of the calculations in the vdW region and created an analytic potential over the whole range by combining the *ab initio* data for the repulsive wall with dispersion-force estimates for the long-range potential and empirical estimates for the well region. Some values calculated from the analytic representation so obtained are also shown in Fig. 1, and we see that they are in better agreement with the present calculations. (It is particularly encouraging that the long-range tail of the present calculations agrees so well with the previous empirical estimates.) The strategy of the present paper is different from that of Ref. [3]. In the present case we have improved the calculation enough so that it is more likely to be adequate in the vdW region and we have adjusted the exponential parameter of the diffuse p function on He so that the vdW well depth and location are approximately correct, and in fact are in about as good agreement with the best available experimental estimates as we were able to achieve in the previous study. We believe that this will yield at least as accurate a potential in the region where it first becomes repulsive, e.g. the region between 6 and $7a_0$ in Fig. 1. Now we will fit the *ab initio* data directly without combining it with extra information. A second difference between the new and previous calculations is that the new ones are not restricted to one orientation angle and one vibrational displacement. Thus the *ab initio* data themselves predict the dependence of V_{int} on r and χ, whereas in the previous study the r and χ dependence were consequences of the pairwise additive assumption. The next section presents the present non-pairwise-additive representation.

3. Analytic representation of the potential

For scattering calculations we represent the total potential energy as

$$V(r, R, \chi) = V_{\text{int}}(r, R, \chi) + V_{I_2}(r) \tag{1}$$

where V_{int} is an analytic representation of the calculated interaction potentials and V_{I_2} is a Morse, given in Ref. [3], curve calculated from the parameters tabulated by Huber and Herzberg [21]. In the rest of this section we consider several ways to represent V_{int}. One common method to represent V_{int} is to expand it in terms of Legendre polynomials; thus for $He\text{–}I_2$ we would write

$$V_{\text{int}}(r, R, \chi) = \sum_{\lambda} \tilde{c}_{\lambda}(r, R) P_{\lambda}(\cos \chi). \tag{2a}$$

If one also takes

$$\tilde{c}_{\lambda}(r, R) = \sum_{j} c_{\lambda j}(R)[(r - r_e)/r]^j, \tag{2b}$$

or some other similar expansion for the r coordinate, and fits the $c_{\lambda j}$ to spline functions, the fitting procedure is quite easy. Note that for the vibrational-coordinate expansion in Eq. (2b), we used the variable $(r-r_e)/r$, as proposed by Simons, Parr, and Finlan [25], since a power series in this variable has better behavior at large r than a power series in $(r-r_e)$. One problem with Eqs. (2a) and (2b) is that the Legendre expansion tends to converge very slowly and hence one needs to calculate the interaction potential at a large number of angles to determine the large number of expansion coefficients required to represent the angular dependence for nonspherical molecules. In particular, it is not possible to represent the infinity, when two atoms overlap, simultaneously with other regions with a finite number of terms in Eq. (2a). An advantage of this procedure though is that it can exactly reproduce the input *ab initio* data.

Another method we considered to represent the interaction potential is

$$V_{\text{int}}(r, R, \chi) = V_{\text{int}}^{\text{PA}}(r, R, \chi) + V^{\text{NPA}}(r, R, \chi), \tag{3}$$

where $V_{\text{int}}^{\text{PA}}$ is a pairwise additive term:

$$V_{\text{int}}^{\text{PA}}(r, R, \chi) = V^{\text{P}}(R_1) + V^{\text{P}}(R_2), \tag{4}$$

where R_j is the distance from the atom to the jth atom in the diatom, and V^{NPA} is a non-pairwise-additive correction term. Usually some functional form containing parameters is used for V^{P}, and V^{NPA} is neglected. The parameters are then adjusted to best fit the *ab initio* data. This procedure can involve many arbitrary options since the parameters in V^{P} are usually nonlinear. This method has the advantage that it can describe highly anisotropic interactions, but it does not reproduce exactly the input *ab initio* data.

We may consider various modifications to the above procedures. One problem with using Eq. (3) is in defining V^{P} so it does describe the bulk of the interaction energy in a physical way. We will define our V^{P} by requiring

$$\begin{aligned} V_{\text{int}}(r = r_e, R, \chi = \pi/2) &= V^{\text{PA}}(r_e, R, \chi = \pi/2) \\ &= 2V^{\text{P}}[(0.25\, r_e^2 + R^2)^{1/2}]. \end{aligned} \tag{5}$$

I.e. we define V^{P} as that function which reproduces the *ab initio* data for T-shaped geometries with I_2 at its equilibrium distance. This gives V^{P} on a grid, and we define it everywhere by using

$$V^{\text{P}}(x) = \begin{cases} A \exp(-bx)/x & x < x_2 \\ \text{cubic spline} & x_2 \leq x \leq x_n \\ -C_6 x^{-6} & x > x_n \end{cases} \tag{6}$$

where x_i is a grid point ordered so that $x_i \leq x_j$ if and only if $i \leq j$. The constants A and b are chosen to reproduce the grid values $V^{\text{P}}(x_1)$ and $V^{\text{P}}(x_2)$, and C_6 is given by $-x_n^6 V^{\text{P}}(x_n)$, where x_n is the largest grid point. The cubic spline has continuous first derivatives across x_2 and x_n.

One possible method uses Eq. (3) with V^{PA} defined by Eqs. (4), (5), and (6), and V^{NPA} defined by

$$V^{NPA}(r, R, \chi) = V_{int}(r, R, \chi) - V_{int}^{PA}(r, R, \chi) \tag{7}$$

and represented by functions like those in Eqs. (2). This procedure exactly reproduces the *ab initio* data when splines are used for the coefficients $c_{\lambda i}$, and is quite simple to perform; but we found for He-I_2 that the Legendre expansion for V^{NPA} converges slowly. This method may work better for diatoms with smaller equilibrium bond distances, but we will not consider it further here.

After experimenting with various ways to improve on the above schemes we finally settled on the following method, which involves switching between the pairwise additive potential $V_{int}^{PA}(r, R, \chi)$, defined by Eqs. (4)-(6), and a small-vibration-amplitude potential $V^{SVA}(r, R, \chi)$ as follows

$$V_{int}(r, R, \chi) = s(r) V_{int}^{SVA}(r, R, \chi) + [1 - s(r)] V_{int}^{PA}(r, R, \chi) \tag{8}$$

where

$$s(r) = \operatorname{sech}[\alpha(r - r_e)]. \tag{9}$$

This switching procedure is similar to that employed previously [6b] for an ArH_2 surface. The small-vibration-amplitude potential is then defined by

$$V_{int}^{SVA}(r, R, \chi) = f^c(r, R, \chi)[V_{int}^{PA}(r, R, \chi) + \varepsilon] - \varepsilon \tag{10}$$

where f^c is given by

$$f^c(r, R, \chi) = [V_{int}(r, R, \chi) + \varepsilon][V_{int}^{PA}(r, R, \chi) + \varepsilon]^{-1} \tag{11}$$

and ε is a small number chosen so that the numerator and denominator are positive everywhere. If ε is large enough, the final potential energy surface is not very sensitive to its exact value, and we use ε equal to minus five times the most negative V_{int} of any of the *ab initio* points; this yields $\varepsilon = 16.35$ meV. This procedure gives f^c on a grid of r, R and χ. We determine it everywhere by using

$$f^c(r, R, \chi) = \sum_\lambda \left\{ \sum_i C_{\lambda i}(R)[(r - r_e)/r]^i \right\} P_\lambda(\cos \chi) \tag{12}$$

and

$$C_{\lambda i}(R) = \begin{cases} C_{\lambda i}(R_1) & R \le R_1 \\ \text{cubic spline} & R_1 < R < R_{n+1} \\ \delta_{\lambda 0}\delta_{i0} & R \ge R_{n+1} \end{cases} \tag{13}$$

where R_1 is the smallest distance at which $C_{\lambda i}$ is known, and R_{n+1} is $2R_n - R_{n-1}$, where R_n and R_{n-1} are the largest distances at which the $C_{\lambda i}$ are known. The cubic splice is constrained to have zero first derivatives at R_1 and R_{n+1}. Note that $C_{00}(R)$ is always positive and if desired one could have spline fit $\ln C_{00}(R)$ rather than $C_{00}(R)$.

This small-vibration-amplitude potential itself, i.e. the above procedure with $s(r) = 1$, works quite well for interpolating and extrapolating in the R and χ coordinates, but has problems extrapolating for large deviations of r from r_e. Only the region of r sampled classically by I_2 in its lower vibrational states ($v \leq 4$, v being the vibrational quantum number) is well represented. The reason we used a switching procedure is to avoid problems for higher vibrational quanta. We used α equal to 0.6 a_0^{-1}, for which the r dependence is well behaved at least to the region sampled classically if I_2 has $v = 80$, which is the range of 4.3 to 7.4 a_0.

For even better global fits one should replace $V_{\text{int}}^{\text{PA}}(r, R, \chi)$ in Eq. (8) by the true pair potential and $V_{\text{int}}^{\text{PA}}(r, R, \chi)$ in Eqs. (10) and (11) by a pair potential that better reproduces the *ab initio* data in an average sense, rather than just at $\chi = 90°$. These refinements were not judged necessary for the present work.

Using the above fitting procedure, it is quite easy to assess the convergence of the analytic representation with respect to the number of angles χ and bond displacements used. Figure 2 shows a test of the convergence of the force on the I_2 bond as a function of χ when various numbers of angles and bond displacements are used. The force is evaluated at $r = r_e$ and R equal to the classical turning point when the asymptotic translational energy is 86.7 meV and ℓ, the orbital angular momentum, is zero. The figure shows that the pairwise additive potential of Ref. [3] gives a very similar curve as the present pairwise additive potential. Thus the main difference between the present and previous results is due to the more extensive set of geometries calculated in the present work, as opposed to the methods used for the electronic structure calculations. The main difference between using the pairwise additive potential and the final potential defined by Eq. (8) using all of the *ab initio* data (3 angles and 3 bond displacements) occurs

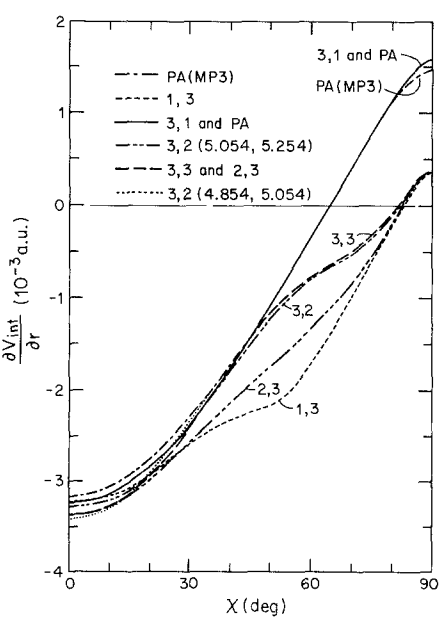

Fig. 2. The force on the I_2 bond at $r = r_e$ and R equals the classical turning point for $\ell = 0$ at a given χ. Several of the curves are labelled n_λ, n_i where n_λ is the number of angles (i.e. the number of λ values) used, and n_i is the number of I_2 bond displacements (i.e. the number of i values) used. The solid curve is for the pairwise additive potential of the present paper, and it is indistinguishable from the potential calculated using 3 angles and 1 vibrational displacement. The long-dashed curve is for 3 angles and 3 vibrational displacements, the long dashed-short dashed curve is for only 0 and 90° but 3 vibrational displacements, the short dashed curve is for only 90° but still 3 vibrational displacements, the long-short-short curve is determined from data at 3 angles with $r = r_e$ and $r =$ 5.254 a_0, the long-short-short-short curve is the same except for $r = r_e$ and $r = 4.854$ a_0, and the long-long-short curve is the pairwise potential based on the MP3 calculations of Ref. [3]

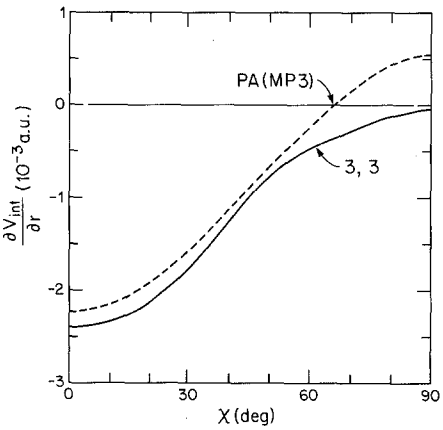

Fig. 3. The same as Fig. 2 except $\ell = 30$ and only the final analytic representation of this paper and the analytic representation of Ref. [3] are shown

for χ greater than about 50°. The potential obtained using all bond displacements but only 0 and 90° [i.e. $\lambda = 0, 2$ in Eq. (12)], differs most from that using all of the *ab initio* data in the range of 30 to 80 degrees. The main effect of adding the 45° data to the fit is to bring the curve very close to the curve using only V_{int}^{PA}. Thus, we conclude that in the range 0 to 50°, the anisotropy of the potential is well converged. If only 90° data is used in the fit, the resulting force is similar to that using 0 and 90°, and for χ less than 25° and greater than 80°, it agrees well with the fit using all of the *ab initio* data. If the number of vibrational displacements used is decreased to two while all three angles are used, the force is very similar to that obtained from the fit using all of the *ab initio* data; thus the vibrational dependence of the potential seems reasonably well converged. If only one vibrational displacement is used, but all three angles are used, the force is extremely close to the force obtained using only V_{int}^{PA}, and hence this force curve is not shown in Fig. 2. In conclusion, to represent the surface accurately, it appears for this system that at least two bond displacements are required, and three (or more) angles are necessary. Figure 3 shows the forces for $\ell = 30$ using the current potential and the potential of Ref. [3].

4. Scattering calculations

We carried out scattering calculations using the new potential energy surface described in the previous section. The dynamics were treated using the vibrational close-coupling, rotational infinite-order-sudden approximation (VCC/IOS). The calculations are for a total energy of 0.1 eV, which corresponds to a relative translational energy of 0.0867 eV when the initial state is the vibrational-rotational ground state.

The close-coupling equations were solved by R matrix propagation, for 17 evenly spaced χ in the range 0 to $\pi/2$. The vibrational-state expansion of the wave function was truncated to the five lowest vibrational channels for ℓ less than 72 and to only the lowest vibrational state for ℓ in the range 72 to 91. The vibrational matrix elements were calculated using an optimized quadrature scheme employing Gauss-ground-state nodes [26]. We found that 6-point quadrature was sufficient

to converge the final T matrix elements to better than 1%, providing another confirmation of the efficiency of this scheme as reported previously [26]. The other integration parameters used and the number of coupled channels were sufficient to converge the significant T matrix elements to better than 1%. In order to calculate the vibrationally elastic cross sections, we augmented the large ℓ phase shifts with ones calculated using the Born approximation for the phase shift [27] with the long-range form of the potential for each χ, i.e. $V_{\text{int}} \cong -C_6(R_1^{-6}+R_2^{-6})$. At $\ell=91$, the Born phase shifts, as compared to the close coupling ones, are 14% too small at $\chi=0°$ and 10% too large at $\chi=\pi/2$. (The accurate phase shifts vary from 6.0×10^{-2} at $\chi=0°$ to 2.85×10^{-2} at $\chi=90°$ for this ℓ.) The Born phase shifts were calculated up to $\ell=120$.

These procedures, with the exception of the method we used to calculate the vibrational matrix elements and the large-ℓ phase shifts, are the same as previously reported [4]. We also use the methods of Ref. [4] to calculate the rotational state-to-state cross sections.

5. Results and discussion

Table 5 shows the calculated integral cross sections as a function of the final rotational state j' for the first three even rotational states for final vibrational quantum number $v'=0$ and the first sixteen for $v'=1$. These cross sections are denoted $\sigma_{v'j'}$ which is the integral cross section for the transition from the initial state $v=0$, $j=0$ (the vibrational-rotational ground state) to the final state with

Table 5. State-to-state and rotationally summed cross sections at relative translational energy $E_{\text{rel}}=0.087$ eV for initial state $v=0$, $j=0$ and final state v', j'

j'	$\sigma_{v'=0,j'}(a_0^2)$	$\sigma_{v'=1,j'}(a_0^2)$
0	239	0.0880
2	43.4	0.285
4	23.0	0.189
6		0.0524
8		0.0351
10		0.0593
12		0.0525
14		0.0330
16		0.0252
18		0.0232
20		0.0188
22		0.0146
24		0.0124
26		0.0111
28		0.00994
30		0.00894
	$\sigma_0(a_0^2)$	$\sigma_1(a_0^2)$
Sum of all j'	438	0.941

vibrational quanta v' and rotational quanta j'. (All of the results quoted in this paper are for the initial state having $v=0$ and $j=0$.) The vibrationally inelastic cross sections have a maximum as a function of j' at $j'=2$ as compared to $j'=16$ from our previous calculations [4] and $\Delta j \cong 5$ from the experiments of Ref. [1]. Thus the new potential significantly improves the agreement with experiment for this quantity. The vibrationally elastic cross sections are more similar to those obtained in our previous calculations. The other quantity which we can directly compare to experiment is the ratio

$$\frac{\sigma^{e}_{0v'}}{\sigma_a} = \frac{\sum\limits_{j'\leq 4} \sigma_{v'=1,j'}}{\sum\limits_{j'\geq 6} \sigma_{v'=0,j'} + \sum\limits_{\text{all } j'} \sum\limits_{v'>0} \sigma_{v',j'}} \tag{14}$$

This is the quantity that the experiments of Hall et al. [1] would give, with the numerator as a function of energy and the demoninator evaluated at a relative translational energy of 0.4 eV, if all the collision partners for the events they observe had $j=0$ and if the laser bandwidth were a step function with its most probable bandwidth. For the present comparison we neglect the initial j dependence. Hall et al. observed that the denominator did not have strong energy dependence; thus we will evaluate this ratio using only our 0.0867 eV data. Our previous calculations [4] also showed that the denominator was approximately energy independent; in particular the value of the demoninator at 0.0867 eV differed from the interpolated value at 0.400 eV by only 1.3%. Our previous result for the ratio in Eq. (14) was 0.48×10^{-3}, which is about a factor of two smaller than the final [1] experimental result of 0.8×10^{-3}, while our new calculations give 4.2×10^{-3}, which is about a factor of five too high. We will consider three possible reasons why we predict too high a ratio. The first is that the theoretical results must be averaged over initial j states, which experimentally correspond to a 1-2K distribution rather than all $j=0$ assumed here, and over the laser intensity distribution, which determines which j' states are included. Such a complete simulation of the experiment is beyond the scope of this work (since it would require both more extensive quantum mechanical calculations and a better characterization of the experimental conditions). A second possible source of the disagreement of theory and experiment is that the theoretical j' distribution is shifted to slightly too small j' for $v'=1$. If the maximum would occur at slightly larger j', then the numerator in Eq. (14) would be reduced. The regions of the potential which are probably most responsible for the error in the j' distribution are those corresponding to $\chi \cong 10$–$40°$, because, as we shall see below, this is where most of the vibrational excitation occurs, and also those corresponding to $\chi = 60$–$90°$, since this is where the vibrational force appears least well converged and differs the most from just using $V_{\text{int}}^{\text{PA}}$. A third possible reason for the disagreement of the ratio in Eq. (14) with experiment is the overall magnitude of the vibrational force. To the extent that the vibrational force is uniformly overestimated at all χ one would expect a similar j' distribution to the experimental one but a decrease in the cross section summed over j'. If this were the main cause for the overestimate of the ratio in Eq. (14), then, based on the correlation

of the force with the inelastic probabilities as discussed in the next paragraph, it would require a change in the force much greater than the variations with basis set observed in Table 3. It would be interesting to test the sensitivity of the vibrational force to more variations in the basis set, such as the iodine basis, and the method by which electron correlation is included. Such tests would be difficult to interpret, however, if the basis set and CI variations also make a significant difference in the calculated values of r_e and ω_e for isolated I_2. It is important to emphasize though that the ratio of Eq. (14) is much more sensitive to small changes in the vibrational force when these are not in the same ratio at all orientation angles. Thus the ratio of Eq. (14) is overall much more sensitive to the quality of the potential than are the totally rotationally summed cross sections $\sigma_{v'}$. For the present surface, σ_1 is only 25% larger than for the pairwise-additive surface, and σ_0 is only 5% smaller. Thus, the second reason mentioned above appears more important than the third, and we conclude that, in interpreting the disagreement with experiment in Ref. [4], we were right to emphasize the distribution of $v'=1$ states over j'.

In Ref. [4] we showed that, for a pairwise-additive potential energy surface, the probability of $v'=1$ vibrational excitation in a collision at a given χ and with a given ℓ was almost proportional to the square of the vibrational force evaluated at $r=r_e$ at the classical turning point of R for the given χ and ℓ. Two questions that arise are: (i) does this almost linear relation continue to exist for a non-pairwise-additive potential, such as the present one, and (ii) is the proportionality constant the same for the two surfaces or is it a function of overall global surface shape? Fig. 4 shows a plot, for all angles χ at which we performed VCC/IOS calculations, of the probability, $P_{01}^{\ell}(\chi)$, of vibrational excitation ($v=0$ to $v'=1$) as a function of the square of the force $-\partial V/\partial r$, evaluated for a given χ with $r=r_e$ and R equal to the classical turning point, i.e. at the root of

$$E_{\mathrm{rel}}-\ell(\ell+1)/(2\mu R^2)-V_{\mathrm{int}}(r, R, \chi)=0 \tag{15}$$

where E_{rel} is the translational energy of 0.0867 eV. As we observed in Ref. [4], this plot is almost linear. The present calculations give a slope of about 6.8×10^3 a.u. which is very close to the value calculated previously, about 6.4×10^3 a.u.;

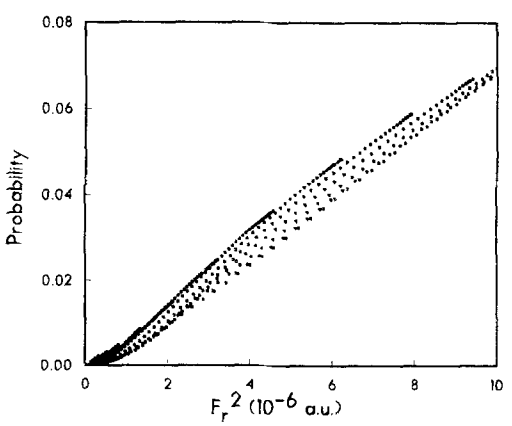

Fig. 4. The probability for vibrational excitation at ℓ and χ as a function of the square of the force ($F_r=\partial V_{\mathrm{int}}/\partial r$) on the I_2 bond when R equals the classical turning point and $r=r_e$

thus the linear relation persists, and the slope is approximately independent of the potential energy surface. This finding is of great import for future *ab initio* studies. It means that, when the goal is to calculate an interaction potential for vibrational excitation calculations, we can concentrate on the vibrational force at a given atom–diatom distance in testing convergence of the electronic structure calculations rather than having to converge the whole interaction potential with less knowledge of which part is most relevant.

Figure 5 shows some state-to-state differential cross sections for the final vibrational state $v' = 1$. These cross sections are backwards peaked, as before [4], but they show much less structure than the ones calculated previously [4].

Figure 6 shows a plot of $\sigma_{v'}(\chi) \sin \chi$ against χ for $v' = 1$. This quantity is related to the cross section for exciting the $v' = 1$ level, summed over all j', by the equation

$$\sigma_{v'} = \tfrac{1}{2} \int_0^{\pi} \sigma_{v'}(\chi) \sin \chi \, d\chi. \tag{15}$$

The main difference in this figure between the curves for the present potential and the pairwise-additive potential of Ref. [3] is the overall scale; the biggest difference in shape occurs near 90°, where the pairwise-additive potential levels to a local maximum about half the height of the maximum at about 25°, whereas the current potential gives almost zero vibrational excitation there. The vanishing of $\sigma_{v'=1}(\chi) \sin \chi$ for the pairwise-additive potential around 65° in Fig. 6 is directly attributable to the zero in the force at this angle in Fig. 2. Similarly the same zeroes shift to about 85° in both plots for the present potential.

Figure 7 shows the opacity as a function of the orbital angular momentum ℓ. The opacity is defined here as the probability of vibration excitation averaged over χ. The results of the current potential are very similar to the results [4] for the potential of Ref. [3].

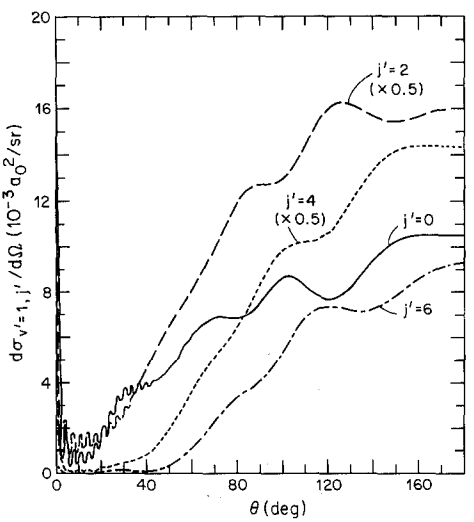

Fig. 5. The differential cross section per unit solid angle as a function of the scattering angle for the transition $v = 0$, $j = 0$ to $v' = 1$, j'. The solid curve is for $j' = 0$, the long dashed curve for $j' = 2$ and is multiplied by 1/2, the short-dashed curve is for $j' = 4$ and is multiplied by 1/2, and the long-short dashed curve is for $j' = 6$

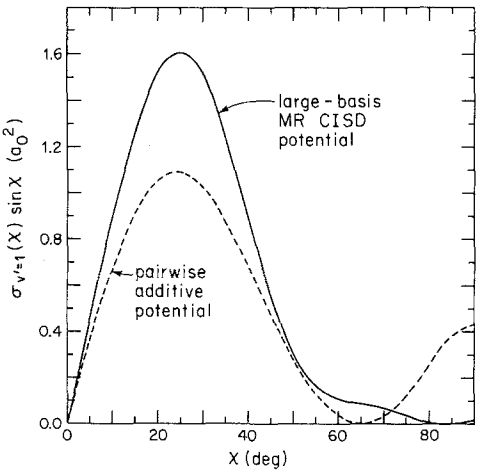

Fig. 6. $\sigma_{v'}(\chi)\sin(\chi)$ for $v'=1$ as a function of χ. The solid curve is from this work, and the dashed curve is from the work of Ref. [4]

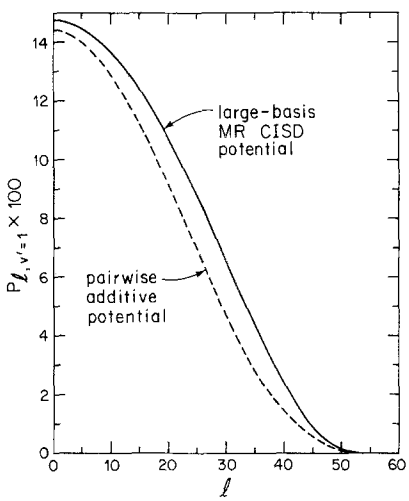

Fig. 7. The opacity as a function of ℓ, the orbital angular momentum, for $v=0$ and $v'=1$. The solid curve is from this work, and the dashed one is from the work of Ref. [4]

6. Conclusions

We have reported a new set of extended-basis-set configuration-interaction (CI) calculations of the He–I_2 interaction potential in the ground electronic state. The calculations include the dependence of the interaction potential on the I_2 orientational angle and vibrational displacement. The orbital set used for the CI calculations is based on a two-configuration SCF calculation that shows proper dissociation in order to avoid the deficiencies of the restricted and unrestricted single-configuration methods as a bond is stretched. The calculations include up to 53 623 configurations and are designed to be as accurate as possible for the force along the I_2 vibrational coordinate at the He–I_2 classical turning point distances of collisions with relative translation energies in the range 50 meV and higher, which is the range of the first available experimental study of vibrational excitation probabilities as a function of collision energy in a neutral system.

We have developed a straightforward method for the analytic representation of interaction potentials for nonreactive collisions of atoms with rotating-vibrating diatoms. The new functional form exactly reproduces all the *ab initio* data at an unlimited set of orientational angles and vibrational displacements, but it does not suffer from the slow convergence of simply expanding the orientation-angle dependence in a Legendre series or from the positive and negative divergences of simply expanding the vibrational-displacement dependence in a power series. One crucial ingredient in the new method is that it builds in the pairwise-additive term, which would require an infinite Legendre series to expand. The vibrational-displacement dependence is handled in the local vicinity of the equilibrium diatom separation by a Simons-Parr-Finlan expansion and is treated globally by switching to a pairwise-additive approximation when the magnitude of the vibrational displacement is large.

We find that the corrections to the pairwise-additive approximation are very important for He-I_2, especially for the vibrational force in highly bent and perpendicular-bisector approach geometries. It is found to be necessary to perform *ab initio* calculations for at least three approach angles and for at least two vibrational displacements.

We performed converged vibrational-close-coupling, infinite-order-sudden-rotation dynamics calculations for the state-to-state cross sections $He + I_2(v=0, j=0) \rightarrow He + I_2(v'=0 \text{ and } 1, j'=0 \text{ to } 30 \text{ or summed})$. The probability of vibrational excitation at a given orientation angle and orbital angular momentum of relative translation is found to correlate almost linearly with the square of the vibrational force at the equilibrium I_2 distance and the classical turning point of the He-I_2 coordinate. Furthermore the proportionality constant depends only slightly on the global form of the potential energy surface. This provides guidance for future *ab initio* calculations because it shows what aspect of the potential energy surface is important to converge.

The most important geometries for vibrational excitation in the present case are found to be those with He off the I_2 axis by about 10-40°. The excitation probabilities in this range are 30-50% higher than for the pairwise-additive potential [3] employed previously [4], but are smaller for orientation angles within 17° of the perpendicular bisector. The net result is that the integral cross section for excitation of $v'=1$, summed over j', is increased 25%. Although this effect is small, the change in shape of the excitation probability, which is clearly correlated with the dependence of the vibrational force on orientation angle at the turning points, makes a much more dramatic change in the j' distribution of vibrationally excited I_2 molecules. We conclude that the experiments of Ref. [1] are much more sensitive to the j' distribution that accompanies $v'=1$ than to the totally rotationally summed $v'=1$ cross section. For a completely satisfactory comparison to experiment one would simulate all j and j' possibilities, but for the present work we were satisfied with an interpretation based on $j=0$ cross sections.

Although the new interaction potential is based on state-of-the-art *ab initio* electronic structure calculations and a faithful analytic representation, the dynamics calculations using it still do not fully account for recent experimental measurements. This is due either to the necessity of using more *ab initio* data in determining the analytic representation of the potential or to deficiencies in the *ab initio* data. In light of the above discussion it would be very interesting to try to determine the vibrational force at the classical turning points more accurately for the orientation angles that make the biggest contributions, namely those differing from collinear by about 20–25°, or for the orientation angles where the forces are most susceptible to interpolation errors in the present scheme, namely orientation angles differing by about 30–35° from perpendicular-bisector approaches.

Acknowledgment. The authors are grateful to P. J. Hay for communicating the ECP for I prior to publication. This work was supported in part by the National Science Foundation through grant number CHE83-17944.

References

1. Hall, G., Liu, K., McAuliffe, M. J., Giese, C. F., Gentry, W. R.: J. Chem. Phys. **78**, 5260 (1983); J. Chem. Phys. **81**, 5577 (1984)
2. For references see the review article; Truhlar, D. G.: Int. J. Quantum Chem. Symp. **17**, 77 (1983)
3. Schwenke, D. W., Truhlar, D. G.: Chem. Phys. Lett. **98**, 217 (1983)
4. Schwenke, D. W., Truhlar, D. G.: J. Chem. Phys. **81**, 5586 (1984)
5. The ODC method was first developed by Das, G. and Wahl, A. C., was reviewed in Adv. Quantum Chem. **5**, 261 (1970). For the cases (I_2 and He-I_2) treated in the present paper the ODC method is equivalent to the generalized valence bond (GVB) method [Hunt, W. J., Hay, P. J., Goddard, W. A.: J. Chem. Phys. **57**, 738 (1972)] and is also sometimes called Hartree–Fock with proper dissociation (HF-PD) [Lie, G. C., Clementi, E.: J. Chem. Phys. **60**, 1275, 1288 (1974)]
6. (a) Duff, J. W., Truhlar, D. G.: J. Chem. Phys. **63**, 4418 (1975); (b) Blais, N. C., Truhlar, D. G.: J. Chem. Phys. **65**, 5335 (1976)
7. Clary, D. C., DePristo, A. E.: J. Chem. Phys. **79**, 2206 (1983); Clary, D. C.: J. Am. Chem. Soc. **106**, 970 (1984)
8. Leutwyler, S., Schmelzer, A., Meyer, R.: J. Chem. Phys. **79**, 4385 (1983)
9. Kahn, L. R., Baybutt, P., Truhlar, D. G.: J. Chem. Phys. **65**, 3826 (1976)
10. Phillips, J. C., Kleinman, L.: Phys. Rev. **116**, 287 (1959)
11. Hay, P. J., Wadt, W. R., Kahn, L. R.: J. Chem. Phys. **68**, 3059 (1978)
12. Christiansen, P. A., Lee, Y. S., Pitzer, K. S.: J. Chem. Phys. **71**, 4445 (1979)
13. Wadt, W. R., Hay, P. J.: J. Chem. Phys. **82**, 284 (1985)
14. Cowan, R. D., Griffin, D. C.: J. Opt. Soc. Am. **66**, 1010 (1976)
15. Kahn, L. R., Hay, P. J., Cowan, R. D.: J. Chem. Phys. **68**, 2386 (1978)
16. Shavitt, I., in: Methods of Electronic Structure Theory, Vol. 1, p. 189, ed: H. F. Schaefer, New York: Plenum 1977
17. Shepard, R., Shavitt, I., Simons, J.: J. Chem. Phys. **76**, 543 (1982)
18. Lischka, H., Shepard, R., Brown, F. B., Shavitt, I.: Int. J. Quant. Chem. Symp. **15**, 91 (1981)
19. Smalley, R. E., Wharton, L., Levy, D. H.: J. Chem. Phys. **68**, 671 (1978)
20. Blazy, J. A., DeKoven, B. M., Russell, T. D., Levy, D. H.: J. Chem. Phys. **72**, 2439 (1980)
21. Huber, K. D., Herzberg, G.: Constants for Diatomic Molecules, Princeton, New York: Van Nostrand 1979

22. Huzinaga, S.: J. Chem. Phys. **42**, 1293 (1965)
23. Meyer, W., Hariharan, P., Kutzelnigg, W.: J. Chem. Phys. **73**, 1880 (1980)
24. Krishnan, R., Binkley, J. S., Seeger, R., Pople, J. A.: J. Chem. Phys. **72**, 650 (1980); Binkley, J. S., Whiteside, R. A., Krishnan, R., Seeger, R., DeFrees, D. J., Schlegel, H. B., Topiol, S., Kahn, L. R., Pople, J. A., GAUSS80, program number QHO3.2, National Resource for Computation in Chemistry Bulletin 3/2, 10 (1980)
25. Simons, G., Parr, R. G., Finlan, J. M.: J. Chem. Phys. **59**, 3229 (1973)
26. Schwenke, D. W., Truhlar, D. G.: Comp. Phys. Commun. **34**, 57 (1984)
27. Baym, G., in: Lectures on Quantum Mechanics, p. 203, New York: Benjamin/Cummings 1978